encit 2020

ABCM Associação Brasileira de Engenharia e Ciências Mecânicas

18th Brazilian Congress of Thermal Sciences and Engineering
November 16–20, 2020 (Online)

ENC-2020-0191
TRANSIENT THERMAL LOAD EVALUATION OF REFRIGERATED CARGO COMPARTMENTS

Igor dos Santos Soares Pinto
Diogo Lôndero da Silva
ReVe-Vehicular Refrigeration Laboratory, Department of Mobility Engineering, Federal University of Santa Catarina, 89219-600, Joinville, SC, Brazil
igor.santos.soares@grad.ufsc.br
diogo.londero@ufsc.br

Abstract. *The transport of refrigerated cargo, as food products, is one of the steps in the cold supply chain and a vital operation for the contemporary society. For instance, in 2019, the Brazilian exports of fresh chilled and frozen beef was responsible for the turnover of US$ 6.546 billion, which represents 3% of the national exports. To maintain the temperature inside the compartment within acceptable levels, without compromising energy consumption targets, the refrigeration system and the cargo compartment must be carefully designed. Moreover, the thermal load of a cargo compartment is also affected by transient ambient conditions, such as external temperature and solar irradiation. For these reasons, this work aims to implement a mathematical model capable of predicting the transient thermal load in refrigerated compartments cargo. The mathematical model is based on the first law of thermodynamics and the fundamentals of heat transfer. It allows to evaluate how the physical and constructive parameters of the refrigerated cargo compartment influence the thermal load, which is required for an energy efficient design. The results show the transient thermal load and energy consumption for different insulation thicknesses and paint absorptivities, showing differences up to 45%. In addition, the mathematical model was used to investigate how different parameters affect the minimal internal temperature achieved by the refrigeration system and its fuel consumption.*

Keywords: *refrigerated cargo compartment, transient thermal load, energy performance*

1. INTRODUCTION

The transport of refrigerated cargo plays a fundamental role in the logistics of supplying perishable foods and items related to the medical field in general, such as pharmaceuticals and blood plasma. For these types of operations, the refrigeration is required to keep the products in good condition and safe for use until arrival at the place of delivery (Bogataj *et al.*, 2005). In 2019, the Brazilian exports of fresh chilled or frozen bovine meat was responsible for a turnover of US$ 6.546 billion, equivalent to 2.9 % of all Brazilian exports (MDIC, 2020). The academic literature has also revealed some important aspects related to on refrigerated cargo transport. For instance, Tso *et al.* (2002) evaluated the effects of heat and mass transfer on the energy consumption of refrigerated trucks. The authors found that the use of air curtains can generate energy savings up to 40%. Da Silva *et al.* (2015) developed a steady state mathematical model to evaluate the energy consumption required to transport refrigerated products, considering geometric and operating parameters. Luchini *et al.* (2018) developed strategy to control the internal temperature of a refrigerated cargo compartment in relation to external thermal disturbances. Artuso *et al.* (2019) proposed a dynamic modeling of a truck's refrigerated cargo compartment during operation and evaluated the peak refrigeration demand. Furthermore, Jara *et al.* (2019) analyzed the thermal behavior of a refrigerated vehicle for food transport, with the purpose of predicting the temperature profile inside the cargo compartment. Despite of the global importance of the refrigerated cargo transport and its huge energy demands, it is observed that few studies have addressed its transient thermal characteristics, which directly influence the quality of the cargo being transported and the energy consumption. Thus, this work aims to implement a mathematical model capable of predicting the transient thermal load of a refrigerated cargo compartment. The mathematical model will be able to evaluate how the physical and constructive parameters of the cargo compartment affect the refrigeration system performance and the internal compartment temperature.

2. REFRIGERATED CARGO DESCRIPTION

A schematic of the vehicle under study is presented in Fig. 1, which shows a truck equipped with a cargo compartment and a refrigeration system. As can be seen, the cargo compartment interacts with two external sources of heat, defined as solar thermal irradiation load ($\dot{Q}_{s,rad}$) and ambient thermal load ($\dot{Q}_{s,amb}$). While part of these two thermal loads is

accumulated on the cargo wall structure, the rest is infiltrated into the compartment, as represented by $\dot{Q}_i$. To maintain the internal temperature of the compartment (T_i), within acceptable values, the infiltrated thermal load ($\dot{Q}_i$) must be removed by the refrigeration system, whose cooling capacity is represented by $\dot{Q}_{refig}$.

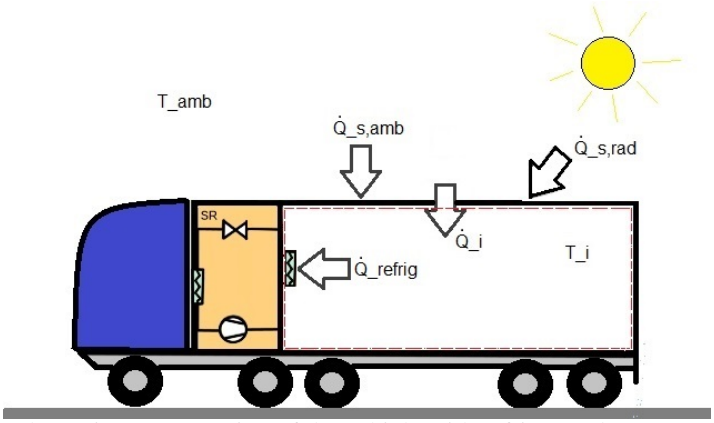

Figure 1: Schematic representation of the vehicle with refrigerated cargo compartment

3. MATHEMATICAL MODEL

The mathematical model presented in this paper is based on ASHRAE (2017) and the work developed by Fayazbakhsh and Bahrami (2013), adopting the necessary simplifications. The mathematical model relays on the first law of thermodynamic, the fundamentals of heat transfer and the following simplifications:

1. Average internal air temperature.
2. Average thermal properties values for each surface element.
3. Uniform temperature across the surface elements.
4. All surfaces with the same insulation thickness.
5. Constant vehicle speed.
6. Vehicle moving from north to south in the south hemisphere.
7. Quasy-static approach for the refrigeration system model.

The geometric inputs of the mathematical model are the vehicle dimensions (length, width and height), thickness of the compartment insulation and the angles of inclination of the compartment surfaces. The operating inputs are time, the speed of the vehicle, the initial temperatures of the compartment, the ambient temperature and the reference temperature for the cargo compartment. On the other hand, the outputs of the model are the thermal load, refrigeration system cooling capacity, power consumption and the temperature inside the compartment. The thermal load components, the refrigeration system and the equations required to evaluate the transient aspects of the problem are described below.

3.1 Thermal load due to solar irradiation

This portion of thermal load is directly related to solar irradiation on surfaces of the refrigerated compartment. As the external surfaces of the compartment are covered by metal sheets, they are considered opaque (zero transmission). Therefore, solar irradiation is firstly absorbed by the compartment walls, causing an increase in the temperature of the surface elements.

The portions of solar radiation that reach the external side of the compartment walls are categorized as direct, diffuse and reflected.

3.1.1 Direct radiation

Portion of radiation received directly from the sun through the sun's rays. Among the three incident radiation plots mentioned above, the one that contributes most significantly is this. The direct solar irradiation, called I_{dir} in this model, is the direct radiation per unit area, given in W/m^2, and is given by the following expression:

$$I_{dir} = \frac{A}{exp(\frac{B}{sen(\beta)})} \tag{1}$$

with A and B being constants defined in ASHRAE (2017) for different months, and β the solar altitude angle, calculated based on the time of day.

3.1.2 Diffuse radiation

Diffuse radiation is related to radiation dispersed in the atmosphere, coming from all directions of the sky. The diffuse solar irradiation, called I_{dif} in this model, is the diffuse radiation per unit area, given in W/m^2, given as a portion of the direct irradiation, by the equation:

$$I_{dif} = CI_{dir}\frac{1 + cos(\gamma)}{2} \tag{2}$$

where C is a constant also defined in ASHRAE (2017) for different months, and γ is the angle between the surfaces and the horizontal.

3.1.3 Reflected radiation

The reflected radiation refers to the portion of radiation that is reflected from the ground and reaches the surfaces of the vehicle compartment. The reflected solar irradiation, named I_{refl} in this model, is the reflected radiation per unit area, given in W/m^2, and is given as a portion of the direct and diffuse irradiations by

$$I_{refl} = (I_{dir} + I_{dif})\rho_g\frac{1 - cos(\gamma)}{2} \tag{3}$$

where ρ_g is the reflectivity coefficient of the ground.

3.1.4 Total solar irradiation thermal load

The total thermal load absorbed by each compartment surface due to the solar irradiation portions is evaluated by

$$\dot{Q}_{s,rad} = S\alpha(I_{dir}cos(\theta) + I_{dif} + I_{refl}) \tag{4}$$

where *S* is the surface element area, α is the surface element absorptivity, and θ is the angle between the normal of the surface under analysis and the position of the sun in the sky.

3.2 Infiltrated thermal load

The infiltrated thermal load considers the conduction heat transfer between the surface elements of the compartment and the internal convection, being described as:

$$\dot{Q}_i = \sum_{sup} SU(T_s - T_i) \tag{5}$$

$$U = \frac{1}{R} \tag{6}$$

$$R = \frac{2\lambda_m}{k_m} + \frac{\lambda_i}{k_i} + \frac{1}{h_i} \tag{7}$$

where U is the total heat transfer coefficient, T_s the external surface temperature and T_i the average internal air temperature of the refrigerated compartment. In Eq. (7), R is the thermal resistance per unity of area and h_i is the internal convective heat transfer coefficient. The parameters λ_m and λ_i are the thicknesses of the metal sheet and the insulation, respectively, while k_m and k_i are the thermal conductivity of the metal sheet and the insulation material. In its turn, the heat transfer between each external surface of the compartment and the environment air was evaluated as

$$\dot{Q}_{s,amb} = Sh(T_{amb} - T_s) \tag{8}$$

where T_{amb} is the external air temperature and *h* is the convective heat transfer calculated by

$$h = 0.6 + 6.64\sqrt{V} \tag{9}$$

as a function of the truck average velocity (*V*).

3.3 Refrigeration system

The mathematical model of the refrigeration system considers a quasy-static approach. It divides the entire process in small time intervals that can be considered in steady state. The refrigeration system is equipped with an externally driven reciprocating compressor produced by Bitzer Compressors (2020). The compressor has a cylinder displacement of 400 cm^3 and operates at 1400 rpm with fluid refrigerant R-404A. The compressor cooling capacity, power consumption and refrigerant mass flow rate were evaluated according to

$$\dot{Q}_{refrig} = \eta_v \dot{m} \Delta h_{evap} \tag{10}$$

$$\dot{W}_{comp} = \eta_s \dot{m} \Delta h_{comp,s} \tag{11}$$

$$\dot{m} = \rho_a V_w \Delta N \tag{12}$$

where η_v is the compressor volumetric efficiency, η_s is the compressor isentropic efficiency, Δh_{evap} is the refrigerant enthalpy change in the evaporator, $\Delta h_{comp,s}$ is the refrigerant isentropic enthalpy change during the compression process, V_w is the compressor displacement, N is the compressor speed and ρ_a is the refrigerant density in the compressor inlet.

The volumetric and isentropic efficiencies were evaluated based on the manufacturer performance curves as

$$\eta_v = c_1 + c_2 \left(\frac{P_d}{P_a} \right)^{\frac{1}{n}} \tag{13}$$

$$\eta_s = \frac{\Delta h_{comp,s}}{\Delta h_{comp}} \tag{14}$$

where P_d is the compressor discharge pressure, P_a is the compressor suction pressure, n is the polytropic coefficient and Δh_{comp} is the real refrigerant enthalpy change during the compression process.

3.4 Energy balances

Applying energy balances on each wall structure of the refrigerated compartment, it is possible to evaluate the derivative of T_s with respect to t as

$$\frac{dT_s}{dt} = \frac{\dot{Q}_{s,amb} + \dot{Q}_{s,rad} - \dot{Q}_i}{m_m c_m + m_i c_i} \tag{15}$$

where $\dot{Q}_{s,amb}$ is the external heat transfer rate due to the temperature difference between the ambient air and the compartment surface, $\dot{Q}_{s,rad}$ is the heat transfer rate due to the solar irradiation, $\dot{Q}_i$ is the heat transfer rate into the compartment, m_m and m_i are the masses of the metal sheets and the insulation material of each wall.

In a similar way, applying an energy balance inside the refrigerated cargo it is possible to evaluate the internal temperature rate of change as

$$\frac{dT_i}{dt} = \frac{\dot{Q}_i - \dot{Q}_{refrig}}{m_a c_a + m_p c_p} \tag{16}$$

where $\dot{Q}_{refrig}$ is the cooling capacity of the refrigeration system and m_a and m_p represents the masses of the air and the cargo inside the compartment, respectively.

3.5 Energy consumption

The energy consumption related to the operation of the refrigeration system (E) is evaluated by

$$E = \frac{\int_0^t \dot{W}_{comp} dt}{\eta_{mec}\eta_{mot}} \tag{17}$$

where η_{mec} is the mechanical efficiency of the compressor and η_{mot} is the efficiency of the combustion engine used to drive the compressor. The total energy consumption is converted in liters or mass of fuel using the energy density of the fuel.

The previous equations were organized in an algorithm and solved with the software *Matlab*. The solution consists in evaluate the thermal loads components for each time step. The numerical integration of differential equations Eq. (15) and Eq. (16) was performed by the method of Runge–Kutta (Kreyszig, 2011).

As can be seen in Fig. 2, after the algorithm receive the geometric parameters and the initial conditions, it evaluates the thermal loads, the refrigeration system power consumption, cooling capacity and predicts the new surfaces and internal temperatures. In each new time step, this new temperatures are used to update the value of the other variables. This iterative procedure is repeated during the entire journey period of the truck.

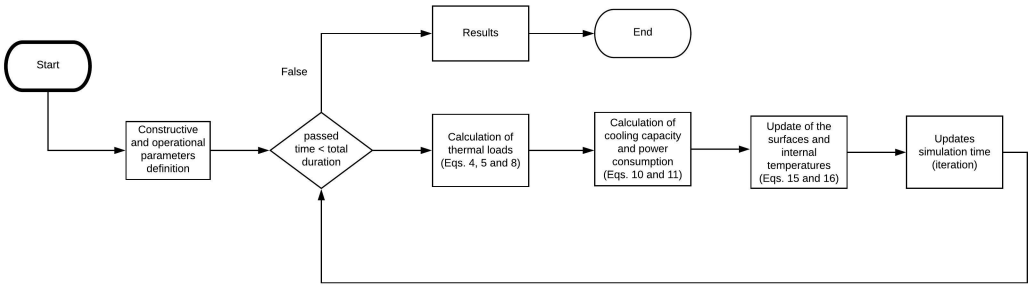

Figure 2: Schematic representation of the solution algorithm

4. RESULTS

The internal volume of the refrigerated compartment under investigation ranges from 38.23 to 43.12 m^3, depending on the thickness of the insulation walls, while the external dimensions of the cargo compartment are fixed and presented in Tab. 1. The compartment walls are comprised by a thermal insulation core protected with metal sheets on the external and internal sides. The insulation material used in this study is expanded polyurethane. Four thicknesses of insulation were considered during the simulations, as presented on Tab. 3. The thickness of the external and internal metal sheets, made of aluminum, were considered equal to 1 mm for all cases. The six surface elements of the refrigerated cargo are considered to calculate the total thermal load. However, due to the north-south journey orientation, it is assumed that only the side and the ceiling walls of the compartment are under the direct irradiation action, with the other surfaces only receiving the diffuse and reflected solar irradiation.

Table 1: Refrigerated compartment external dimensions

Dimensions	Measures [m]
Length	7.5
Width	2.4
Height	2.6

Table 2: Refrigerated compartment insulation thicknesses

Case	Thickness [mm]
Insulation 1	50.0
Insulation 2	80.0
Insulation 3	100.0
Insulation 4	120.0

Before using the mathematical model to investigate the proposed problem, the effect of the size of the time step was evaluated. This analysis is necessary to define the proper time step used during the simulations. Figure 3 shows the evolution of the compartment's internal temperature, for different time steps sizes. It is observed that time steps of 150, 120, 60 and 30 seconds presented differences larger than 20 °C between their curves, which are unacceptable for this kind of study. As the time step is reduced, the curves start to have similar trends. In particular, the time step curves of 10, 5 and 2 seconds have very close values, since the beginning of the simulation. Based on these results, the time step chosen for the simulations was 10 seconds, as it allows calculations with good precision and acceptable computational expense.

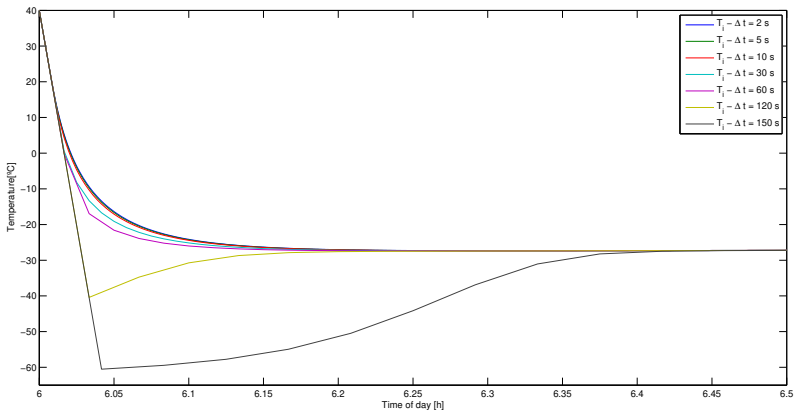

Figure 3: Effect of the time step size in the refrigerated cargo internal temperature

Figure 4 shows, for different insulation thicknesses, the internal temperature evolution of the compartment over time with the cooling system switched off, the vehicle stopped and an empty compartment ($m_p = 0$). The simulation was initiated at 5 h assuming a critical condition in which the internal and external air temperatures were in equilibrium at 40 °C. It is possible to notice that there is a symmetry in the internal air temperature profile, with the center of the curve around noon. This is due to the lateral and roof surfaces symmetrically receiving solar irradiation throughout the day. At around 10:00 h and 15:00 h, the internal temperature peaks, of approximately 57 °C, are noted. This behavior can be explained by Eq. (4), that results in a maximum of direct irradiation for these times.

In addition, Fig. 4 shows a difference in the temperature curves for each insulation thickness. For example, it is observed that the internal temperature related to the insulation of 120 mm takes longer to reach its peak than the other cases, of smaller thicknesses. These different results show that mathematical model is sensible to differences on the characteristics of the insulating material.

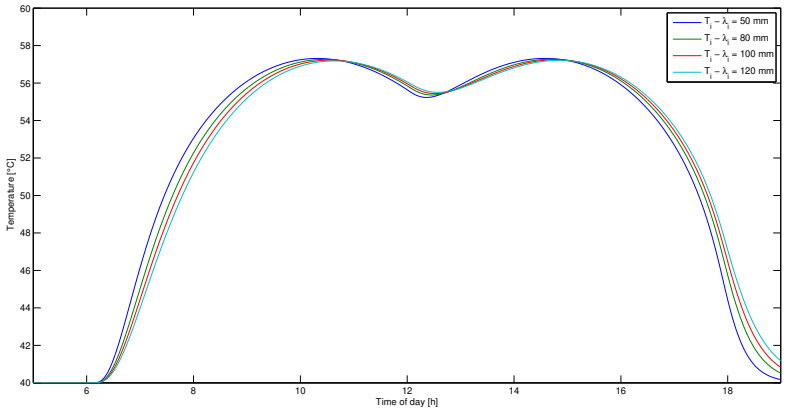

Figure 4: Internal temperature of the compartment for different insulation thickness with the cooling system switched off

The simulations were also performed with the refrigeration system switched on and the truck in motion. The vehicle velocity was fixed at 20 m/s to evaluate the external heat transfer convection coefficient (Eq. (9)). For this condition, Fig. 5 shows the infiltrated thermal load ($\dot{Q}_i$) as a function of time, for different insulation thicknesses. As can be seen, the greater the thickness of the insulation, the lower is the infiltrated thermal load. These results are consistent with Eq. (5), since the increase in the thickness of the compartment insulation (λ_i) results in the U decrease. In all cases, the infiltrated thermal load oscillates over time due to the change in the relative position of the sun. The peaks in the thermal

load are also observed around 10:00 h and 15:00 h, when a large external area, from the top and side of the compartment, is exposed to the direct solar irradiation. Although the solar irradiation achieve its maximum at noon, only the top area is affected by this component at this time.

The maximum infiltrated thermal load values are 3950 W for 50 mm insulation, 2890 W for 80 mm insulation, 2470 W for 100 mm insulation and 2190 W for 120 mm insulation. As can be seen, a reduction in the infiltrated thermal load around 45% can be achieved by increasing the thermal insulation thickness. In addition, Fig. 5 shows that the infiltrated thermal load amplitude is reduced by increasing the insulation thickness. For instance, the differences between the maximum and minimum values are 250 W and 90 W for the insulation thicknesses of 50 mm and 120 mm, respectively.

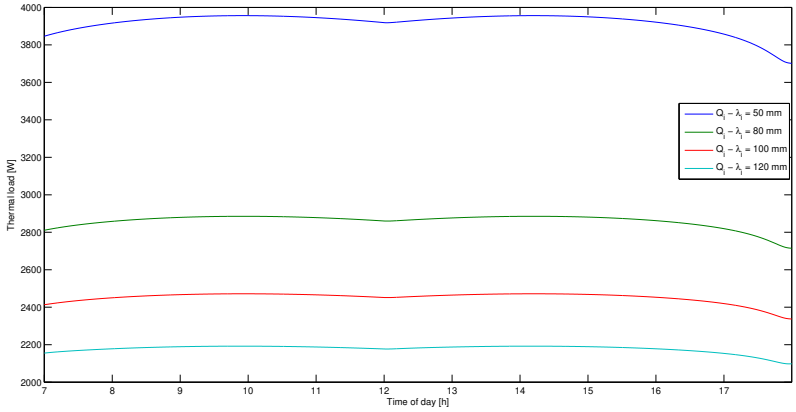

Figure 5: Transient infiltrated thermal load for different insulation thicknesses

Figure 6 shows the the refrigeration system cooling capacity as a function of time, for different insulation thicknesses. A comparison between Fig. 5 and Fig. 6 shows that the magnitudes of the infiltrated thermal load and the refrigeration cooling capacity are affected in a similar way by the insulation thicknesses. However, Fig. 7, which compares $\dot{Q}_{refrig}$ and $\dot{Q}_i$ for λ_i = 50 mm, shows that there is a lag between this two variables. This is due to the infiltrated thermal load parcel that is accumulated on the interior of the refrigeration compartment structures and air, before being removed by the refrigeration system.

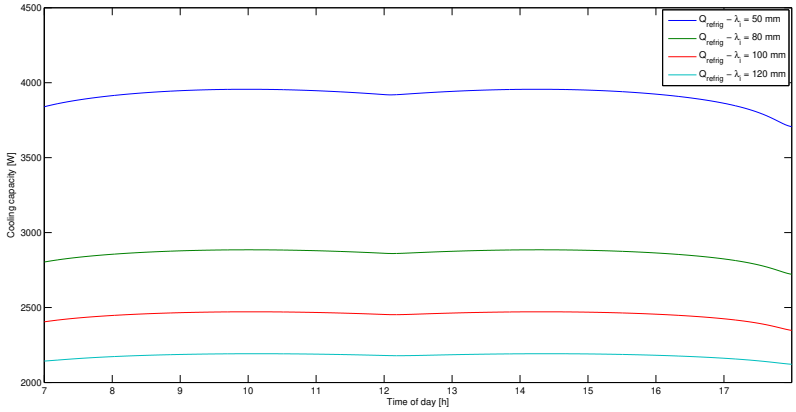

Figure 6: Transient cooling capacity for different insulation thicknesses

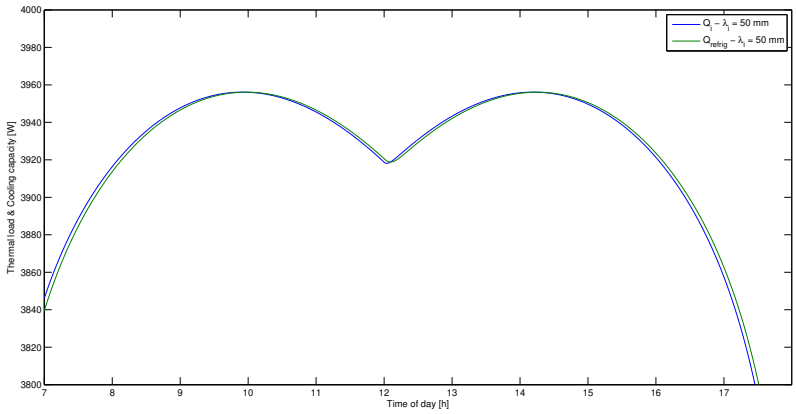

Figure 7: Comparison between infiltrated thermal load and system cooling capacity over the time

The internal temperature of the refrigerated compartment, when the refrigeration system is switched on, was also evaluated. In order to consider the critical condition, the mathematical model was used to evaluated the minimal internal temperatures related to the peaks in the infiltrated thermal load, identified at 10:00 h in Fig. 5. As can be seen in Fig. 8, the increase of the insulation thickness allows the refrigerated compartment operate at lower internal temperatures. For instance, the values of the minimum internal temperatures are -26.4 °C and -38.1 °C for insulation thickness of 50 mm and 120 mm, respectively. Moreover, if a setpoint temperature of -30 °C were required for the transported product, the refrigerated cargo designed with 50 mm of insulation will not be able to achieve the desired internal temperature.

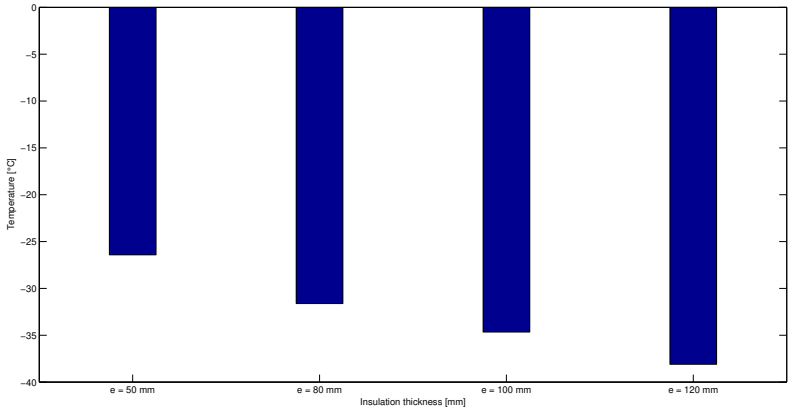

Figure 8: Minimal internal temperatures for different insulation thicknesses at maximum infiltrated thermal load

The mathematical model was also used to evaluate different paint absorptivities on the refrigerated compartment thermal transient performance. Figures 9a and 9b show the influence of paint absorptivity on the the cooling capacity and the internal temperature, respectively. As can be seen, the increase in the absorptivity of the paint, α, from 0.30 (white zinc oxide paint) to 0.98 (black paint), changes the required cooling capacity and the internal temperature. Considering a insulation thickness of 50 mm, the peak cooling capacity is approximately 3890 W for α = 0.3, while it is equal to 4335 W for α = 0.98. This change represents an increase of 11.39 %. For an insulation thickness of 120 mm, the observed peak cooling capacity is 2190 W for α = 0.30, and 2350 W for α = 0.98, which represents an increase of about 7.35 %. Thus, it is noted that compartments with greater insulation thickness suffer less influence of the paint absorptivity.

As the paint absorptivity changes the thermal load and the cooling capacity, the internal temperature is also affected. Figure 9b shows that, for 50 mm of insulation, the internal temperature peak is increased from -26.5 °C to -25 °C due to the ink absorptivity difference. For 120 mm of insulation, the internal temperature peak is increased from -38.5 °C to -35.9 °C. These results also show that the internal temperature change is not linearly related with the insulation thickness. This behavior is mainly justified by the volumetric efficiency of the compressor (Eq. (13)), that is reduced with the refrigerated cargo internal temperature. Therefore, it is observed that the paint absorptivity used on the surfaces of refrigerated compartments has a considerable influence on the required cooling capacity and the related internal temperatures.

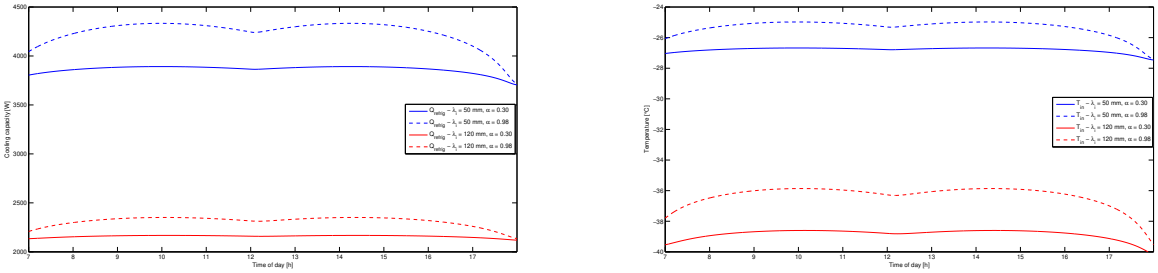

(a) (b)

Figure 9: Effect of the paint absorptivity on the (a) system cooling capacity and (b) internal temperature for different insulation thicknesses

Figure 10a compares the evolution of the refrigeration system power consumption for different insulation thicknesses. It is observed that the greater the thickness of the thermal insulation, the lower the power consumed by the cooling system. The peak power consumption values are observed at 10:00 and 15:00 h, due to the maximum absorbed solar irradiation. For instance, at these peaks, the observed power consumption is 1500 W and 835 W for the insulation thicknesses of 100 mm and 120 mm, respectively, which represents a difference of 44 %. The effect of the surface paint absorptivity on the power consumption is also observed in Fig. 10b. As can be seen for a insulation thickness of 50 mm, the paint absorptivity change from 0.30 to 0.98 results in an increase in the maximum values of power consumption from 3000 W to 3250 W. This represents an increase of 8 % on the power consumption.

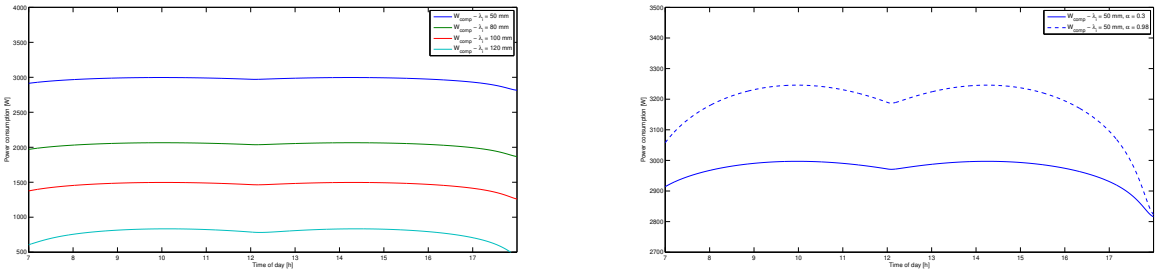

(a) (b)

Figure 10: (a) System power consumption for different insulation thicknesses and (b) influence of painting absorptivity in the system power consumption, for the insulation thickness of 50 mm

Finally, the influence of the insulation thickness and the paint solar absorptivity on the energy consumption of the system was quantified. For the analysis, it was considered $\eta_{mec} = 0.95$ and $\eta_{mot} = 0.30$ (Sonntag *et al.*, 2008). Moreover, the amount of energy per liter of diesel was considered equal to 3.6 10^7 J/liter (EDUS, 2015). Table 3 compares the energy and the amount of diesel consumed for insulation thicknesses of 100 and 120 mm. It is noted that the increase of the thermal insulation thickness from 100 mm to 120 mm reduces the fuel consumption in 45 %. In addition, Table 4 compares the energy and diesel consumption considering 50 mm of insulation thichness and different paint properties. As can be seen, the change of the paint absorptivity from 0.30 to 0.98 results in an increase of 1 liter of diesel, that represents a difference of 8 % for this case. These results show that the insulation thickness has a larger effect than the paint absorptivity on the energy consumption.

Table 3: Total energy and fuel consumption for the cases of insulation thicknesses of 100 and 120 mm

Cases	Total energy consumed [J]	Diesel consumed [l]
$\lambda_i = 100\ mm$	2.2 10^8	6.2
$\lambda_i = 120\ mm$	1.2 10^8	3.4

Table 4: Energy and fuel consumption for the painting absorptivities of 0.30 and 0.98, and insulation thickness of 50 mm

Cases	Total energy consumed [J]	Diesel consumed [l]
$\lambda_i = 50\ mm, \alpha = 0.30$	$4.5\ 10^8$	12.4
$\lambda_i = 50\ mm, \alpha = 0.98$	$4.8\ 10^8$	13.4

5. CONCLUSIONS

This work presents a mathematical model to evaluate the transient thermal loads in a typical vehicle compartment used to transport refrigerated cargo. The mathematical model is based on the first law of thermodynamics and the fundamentals of heat transfer. It takes into account geometric parameters and operating conditions, including the solar irradiation, to evaluate the transients in the infiltrated thermal load, the cooling capacity and power consumption of the refrigeration system and the air temperature inside the cargo compartment. The infiltrated thermal load was evaluated, with the refrigeration system switched on, indicating a difference of 45 % on the thermal load for different insulation thickness. Thermal load peaks at 10:00 h and 15:00 h hours were observed due to the transient characteristic of the direct solar irradiation parcel. The results also show a reduction in the infiltrated thermal load amplitude related to insulation thickness increase. It was observed that the insulation thickness affects the minimal internal temperatures reached by the refrigeration system. The results show that the minimal internal temperature can be reduced in $11^{\circ}\mathrm{C}$ by increasing the insulation thickness from 50 mm to 120 mm. Finally, the mathematical model was used to evaluate the refrigeration system energy and fuel consumption. The analysis showed that the insulation thickness have a larger effect than the paint absorptivity on the fuel consumption.

6. REFERENCES

Artuso, P., Rossetti, A., Minetto, S., Marinetti, S., Moro, L. and Del Col, D., 2019. "Dynamic modeling and thermal performance analysis of a refrigerated truck body during operation". *International Journal of Refrigeration*, Vol. 99, pp. 288–299.

ASHRAE, 2017. "ASHRAE - Handbook Fundamentals". *American Society of Heating, Refrigerating and Air-Conditioning Engineers, Atlanta : ASHRAE*.

Bitzer Compressors, 2020. "Compressors for transport applications (Truck and Trailers)". URL `https://www.bitzer.de/br/pt-br/transporte/truck-n-trailer/`.

Bogataj, M., Bogataj, L. and Vodopivec, R., 2005. "Stability of perishable goods in cold logistic chains". *International journal of production economics*, Vol. 93, pp. 345–356.

Da Silva, D.L., Silva, V.M.D. and de Sena Taglialenha, S.L., 2015. "Um modelo matemático para a análise energética do transporte terrestre de cargas refrigeradas".

EDUS, 2015. "Properties of Fuels, Energy Efficiency and Renewable Energy". Technical report, United States Department of Energy.

Fayazbakhsh, M.A. and Bahrami, M., 2013. "Comprehensive modeling of vehicle air conditioning loads using heat balance method". Technical report, SAE Technical Paper.

Jara, P.B.T., Rivera, J.J.A., Merino, C.E.B., Silva, E.V. and Farfán, G.A., 2019. "Thermal behavior of a refrigerated vehicle: Process simulation". *International Journal of Refrigeration*, Vol. 100, pp. 124–130.

Kreyszig, E., 2011. *Advanced Engineering Mathematics*. John Wiley & Sons, Inc., 10th edition.

Luchini, E., Radler, D., Ritzberger, D., Jakubek, S. and Kozek, M., 2018. "Model predictive temperature control and ageing estimation for an insulated cool box". *Applied Thermal Engineering*, Vol. 144, pp. 269–277.

MDIC, 2020. "Data on the brazilian foreign trade of chilled and frozen beef during 2019". URL `http://comexstat.mdic.gov.br/pt/comex-vis`.

Sonntag, R.E., Van Wylen, G.J. and Borgnakke, C., 2008. *Fundamentals of thermodynamics*. Wiley, 7th edition.

Tso, C., Yu, S., Poh, H. and Jolly, P., 2002. "Experimental study on the heat and mass transfer characteristics in a refrigerated truck". *International Journal of Refrigeration*, Vol. 25, No. 3, pp. 340–350.